Vessel Enhancing Diffusion

A Scale Space Representation of Vessel Structures

Rashindra Manniesing [a,*], Max Viergever [a], Wiro Niessen [b]

[a] *Image Sciences Institute, University Medical Center Utrecht, Heidelberglaan 100, 3584 CX Utrecht, the Netherlands*

[b] *Biomedical Imaging Group Rotterdam, Erasmus MC - University Medical Center Rotterdam, Departments of Medical Informatics and Radiology, Dr. Molewaterplein 50, 3015 GE Rotterdam, the Netherlands*

Abstract

A method is proposed to enhance vascular structures within the framework of scale space theory. We combine a smooth vessel filter which is based on a geometrical analysis of the Hessian's eigensystem, with a nonlinear anisotropic diffusion scheme. The amount and orientation of diffusion depend on the local vessel likeliness. Vessel enhancing diffusion (VED) is applied to patient and phantom data and compared to linear, regularized Perona-Malik, edge and coherence enhancing diffusion. The method performs better than most of the existing techniques in visualizing vessels with varying radii and in enhancing vessel appearance. A diameter study on phantom data shows that VED least affects the accuracy of diameter measurements. It is shown that using VED as a preprocessing step improves level set based segmentation of the cerebral vasculature, in particular segmentation of the smaller vessels of the vasculature.

Key words: scale space, nonlinear anisotropic diffusion, vessel enhancing diffusion (VED), computed tomography angiography (CTA)

1 Introduction

Vessel analysis in medical images is important both for diagnostic and intervention planning purposes. Vessel centerline extraction can be used to generate

* Corresponding author. Tel.: +31 30 2507772, fax: +31 30 2513399
Email addresses: rashindra@isi.uu.nl (Rashindra Manniesing), max@isi.uu.nl (Max Viergever), w.niessen@erasmusmc.nl (Wiro Niessen).

specific visualizations, such as endovascular views or multiplanar reformats. Vessel segmentation can be used for quantification, e.g. for stenosis grading, or to determine the dimension of stents to be used in interventions. In many approaches for vessel analysis, images are first preprocessed to enhance vascular structures. Vessel enhancement improves vessel visualization, e.g. in volume rendering techniques or maximum intensity projections, and has the potential to facilitate the task of centerline extraction and segmentation.

In this paper a method is proposed to enhance vascular structures within the framework of scale space theory. In scale space theory, a family of images is generated by evolving the image according to the diffusion equation $L_t = \nabla \cdot (D \nabla L)$, with the original image as the initial condition. The diffusion tensor D enables us to control the flow such that features of interested are blurred or preserved. The simplest form is by taking the identity matrix for D that results in the heat equation. The first nonlinear (isotropic) variant was proposed by Perona and Malik (1990), in which the diffusion tensor is replaced by a scalar function of the gradient magnitude. Weickert (1996a, 1999) went one step further by using the orientation to enhance small edges and coherent structures by analyzing the structure tensor of the image, obtaining anisotropic behavior. For an overview we refer to (ter Haar Romeny, 1994) and (Weickert, 1997). In this work we replace the diffusion tensor by a function of the Hessian. The eigensystem of the Hessian have direct geometrical interpretation which can be used to construct a vesselness measure, such as described in (Koller et al., 1995; Lorenz et al., 1997; Sato et al., 1998; Frangi et al., 1998; Krissian et al., 2000) and which can be used to steer the diffusion.

We have found only a few works similar to ours, namely (Cañero and Radeva, 2003) and (Krissian, 2002). In (Cañero and Radeva, 2003) a vesselness measure is used to steer the diffusion process. An important difference is that the tensor function we propose satisfies a smoothness constraint; a necessary condition imposed by the diffusion process to ensure it is well-posed. The second difference is related to the steering of the diffusion. Instead of having small diffusion for non-vessel structures we have strong isotropic diffusion to reduce background noise, and, in between the extremes of isotropic and anisotropic diffusion, a parameter is introduced to adjust the sensitivity on the vesselness response. Furthermore, compared to (Cañero and Radeva, 2003), the method is extended to 3D. In (Krissian, 2002) the minimal principal curvature direction of the isosurface is used to steer the diffusion, which requires the calculation of the gradient vector field. This may pose a problem along the central vessel axis as the gradient vanishes at these points, possibly leading to undesired behavior. In our approach we use the full eigensystem of the Hessian which is defined across the entire vessel.

This paper is organized as follows. The underlying theory is described in Section 2, the experimental framework is described in Section 3. The method is

applied to phantom data and patient data of the human cerebral vasculature, and is evaluated with respect to visualization (Sections 4 and 5), diameter quantification (Section 6) and segmentation (Section 7). Finally, discussion and conclusions are presented in Section 8.

2 Method

2.1 Diffusion Filter Class

It has been shown that under fairly mild conditions on the diffusion tensor, the diffusion equation is well-posed, regular and satisfies a minimum-maximum principle. Well-posed means that the problem has a solution which is unique and continuously depends on the initial image. Regular implies that the solution belongs to the class of smooth functions. The extremum principles states that the range of intensity values becomes smaller - in fact, the intensity range converges to the average gray value of the image if the number of iterations goes to infinity. The derivation can be found in (Weickert, 1999, 1996a) where the results from (Catté et al., 1992) and (Weickert, 1996b) are generalized. Here, only the three conditions imposed on the diffusion tensor $D = (d_{ij})$ are given, which are repeated from (Weickert, 1999):

Smoothness $D \in C^{\infty}(\mathbb{R}^{m\times m}, \mathbb{R}^{m\times m})$ with m denoting the dimension.
Symmetry $d_{ij}(H) = d_{ji}(H)$ for all symmetric matrices $H \in \mathbb{R}^{m\times m}$.
Uniformly Positive Definite Let $\Omega \in \mathbb{R}^m$ be the open, bounded subset of $\mathbb{R}^m$ denoting the image domain, let $\overline{\Omega}$ be the closure of Ω and let $K \in \mathbb{R}$. Then, for all $w \in L^{\infty}$ with $w : \Omega \to \mathbb{R}$ that satisfy $|w(x)| \leq K$ on $\overline{\Omega}$, there exists a positive lowerbound $\upsilon(K)$ for the eigenvalues of $D(H)$.

We aim at constructing a tensor D which fulfills these requirements and allows for vessel preserving diffusion. This enables the construction of a multiscale representation of vascular imaging data, that possesses desirable scale space properties and hence could effectively be used for multiscale approaches to vascular image analysis.

2.2 Vesselness Filter

In order to tune the diffusion process to vascular structures in the image, we analyze the eigensystem of the Hessian matrix $\mathcal{H}$. The eigenvectors point in the direction in which the second order image information takes extremal values, the eigenvalues give these extremal values. We call these the curvature

directions and curvatures [1].

In the case of bright vessels on a dark background, and with the following ordering of eigenvalues $|\lambda_1| \leq |\lambda_2| \leq |\lambda_3|$, the direction along the vessel is given by v_1 when $|\lambda_1| \approx 0$ and $|\lambda_1| \ll |\lambda_2| \approx |\lambda_3|$. Several vesselness filters have been proposed based on the eigenvalues of the Hessian (Lorenz et al., 1997; Sato et al., 1998; Frangi et al., 1998; Krissian et al., 2000). Our definition of a vesselness function is based on the work of Frangi et al. (1998). This function consists of exponential functions, which turns out to be advantageous when modifying the function to satisfy the constraints imposed on the diffusion tensor to generate a scale representation as stated in Section 2.1. The formulation of the vesselness measure by Frangi et al. (1998), is as follows:

$$\mathcal{V}_F(\vec{\lambda}) \triangleq \begin{cases} 0 & \text{if } \lambda_2 > 0 \text{ or } \lambda_3 > 0 \\ \left(1 - e^{-\frac{A^2}{2\alpha^2}}\right) \cdot e^{-\frac{B^2}{2\beta^2}} \cdot \left(1 - e^{-\frac{S^2}{2\gamma^2}}\right) & \text{otherwise} \end{cases} \tag{1}$$

with

$$A = \frac{|\lambda_2|}{|\lambda_3|} \tag{2}$$

$$B = \frac{|\lambda_1|}{\sqrt{|\lambda_2 \lambda_3|}} \tag{3}$$

$$S = \sqrt{\lambda_1^2 + \lambda_2^2 + \lambda_3^2} \tag{4}$$

in which A differentiates between plate and line like structures, B accounts for deviation from a blob like structure, and S differentiates between foreground (vessel) and background (noise). The parameters α, β and γ are weighting factors determining the influence of A, B and S. The vesselness response is calculated at multiple scales by computing the Hessian with Gaussian derivatives at multiple scales. At every voxel location, the vesselness output with the highest response is selected.

2.3 Smoothed Vesselness Filter

Unfortunately, the vesselness function $\mathcal{V}_F$ is not smooth at the origin, and therefore can not directly be used to construct a vesselness diffusion equation. Smoothness implies that the nth-order derivative exists and is continuous. The following modifications are proposed to remedy this issue. The first modification applies to the domain definition: by setting the vesselness to zero for

[1] To be distinguished from the isophote and isosurface curvature measures.

$\lambda_{\{2,3\}}$ larger than or equal to zero, the function becomes continuous at the limit $\vec{\lambda} \to \vec{0}$. Still, the resulting function is not smooth, which is due to the ratio of polynomial functions in λ_i. Suppose $\lambda_2 = \lambda_3 \triangleq \alpha\lambda_1$ with $\alpha \in \mathbb{R}$ and $\alpha \geq 1$ and consider $\lambda_1 \to 0$. This results in $\partial^2\mathcal{V}_F/\partial\lambda_1^2 = (2+4\alpha^2)(1-1/e)e^{(-1/\alpha^2)}$. A similar argument can be applied in the 2D case for the first order derivative in λ_1; thus the diffusion tensor proposed in (Cañero and Radeva, 2003) is not smooth either. To resolve this non-smoothness problem, observe that $\mathcal{V}_F$ and $\mathcal{V}_F^{(n)}$ consist of terms of the form

$$T(\vec{\lambda}) = \left(\frac{P}{Q}\right) e^{-\left(\frac{R}{S}\right)} \tag{5}$$

with $\{P, Q\}$ polynomial functions in $\vec{\lambda}$, and $\{R, S\}$ polynomial functions in $\vec{\lambda}$ without any constant terms. Obviously, $\{R, S\}$ remain the same for any order derivative, only $\{P, Q\}$ change. If $\vec{\lambda} \to \vec{0}$ then $\{R, S\} \to \{0, 0\}$, making T undefined. Multiplying T with $e^{(-1/S)}$ gives

$$\left(\frac{P}{Q}\right) e^{-\left(\frac{R+1}{S}\right)} \tag{6}$$

which always goes to zero if $\vec{\lambda} \to \vec{0}$, making this new term properly defined around the origin. By collecting the exponential terms of $\mathcal{V}_F$, it immediately follows that the smallest common denominator is $|\lambda_2|\lambda_3^2$. Therefore, multiplying $\mathcal{V}_F$ with

$$e^{-\left(\frac{2c^2}{|\lambda_2|\lambda_3^2}\right)} \tag{7}$$

with c some constant, will result in a smoothed version of the vesselness function. It resembles a Gaussian function with its argument inverted, and it is controlled by the standard deviation c. This constant c should be chosen very small to only have influence around the origin. The new vesselness function $\mathcal{V}_s$ then reads

$$\mathcal{V}_s(\vec{\lambda}) \triangleq \begin{cases} 0 & \text{if } \lambda_2 \geq 0 \text{ or } \lambda_3 \geq 0 \\ \left(1 - e^{-\frac{A^2}{2\alpha^2}}\right) \cdot e^{-\frac{B^2}{2\beta^2}} \cdot \left(1 - e^{-\frac{S^2}{2\gamma^2}}\right) \cdot e^{-\frac{2c^2}{|\lambda_2|\lambda_3^2}} & \text{otherwise} \end{cases} \tag{8}$$

with range $\mathcal{V}_s \in [0, 1]$. Similarly to the original vesselness function, a multiscale approach is adopted, *i.e.* the Hessian $\mathcal{H}$ is calculated by second order Gaussian derivatives at multiple scales - each normalized by σ^2 (Lindeberg, 1998), and

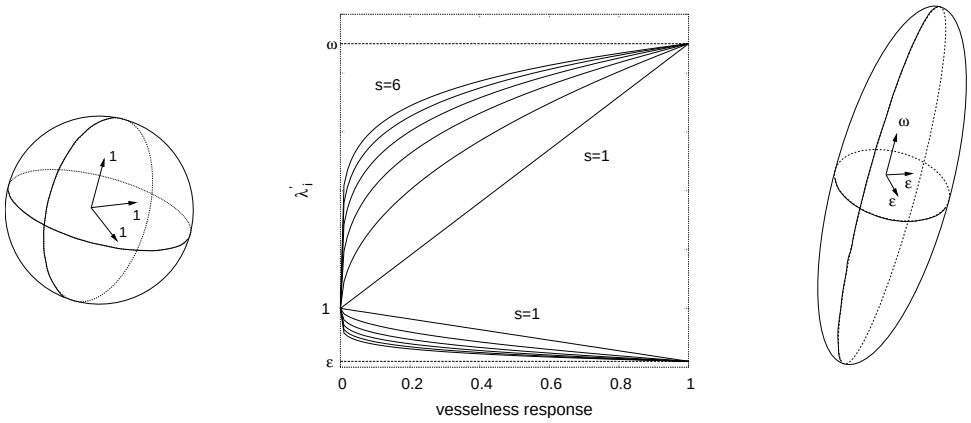

Fig. 1. The eigenvalues of the diffusion tensor D are functions of the vesselness function $\mathcal{V}$. If the vesselness is zero, isotropic diffusion takes place which is represented by the sphere, if the vesselness is one, anisotropic diffusion takes place which is represented by the ellipsoid. In between, a continuous transition is possible with parameter s specifying the sensitivity on $\mathcal{V}$. In the graph, the functions are drawn for $s > 1$; λ'_1 (Equation 11) is given by the curves above the line $y = 1$ and $\lambda'_{\{2,3\}}$ (Equation 12) are given by the curves below the line $y = 1$.

the maximum response is selected. At this maximum response the eigensystem of the Hessian is calculated.

$$\mathcal{V} = \max_{\sigma_{min} \leq \sigma \leq \sigma_{max}} \mathcal{V}_s(\vec{\lambda}) \tag{9}$$

2.4 Nonlinear, Anisotropic Vessel Enhancing Diffusion

Based on the new smoothed vesselness function $\mathcal{V}$ (Equation 9) several scale spaces can be constructed, depending on the application of interest. The approach is similar to the work of Weickert who introduced 'edge enhancing diffusion' (Weickert, 1996a) and 'coherence enhancing diffusion' (Weickert, 1999) (these schemes are briefly touched upon in Section 3.2), based on the eigensystem of the structure tensor. The objective here is to construct a scale space that preferably preserves vasculature structures. This can be achieved by defining the diffusion tensor D such that for vessel structures diffusion mainly takes place in the direction along the vessel, while diffusion perpendicular to this direction is inhibited. We therefore propose the following definition for the diffusion tensor

$$D \triangleq Q\Lambda' Q^T \tag{10}$$

with Q the eigenvectors of $\mathcal{H}$ and Λ' having the following functions on its diagonal

$$\lambda'_1 \triangleq 1 + (\omega - 1) \cdot \mathcal{V}^{\frac{1}{s}} \tag{11}$$

$$\lambda'_2 = \lambda'_3 \triangleq 1 + (\epsilon - 1) \cdot \mathcal{V}^{\frac{1}{s}} \tag{12}$$

with $\mathcal{V} \in [0, 1]$ and parameters $\omega > \epsilon$, $\epsilon > 0$ and $s \in \mathbb{R}^+$. Parameter ω should in general be a large value (may be larger than one [2]) and indicates the strength of anisotropic diffusion, parameter ϵ should in general be a very small value, but larger than zero to ensure the positive definiteness of the tensor and parameter s denotes the sensitivity to the vesselness response. The motivation for this diffusion tensor is as follows: for non-vessel structures ($\mathcal{V}$ goes to zero) diffusion is high and isotropic, and background noise is reduced, whereas for vessel structures ($\mathcal{V}$ goes to one) diffusion is maximal (ω) in the minimal curvature direction, *i.e.* along the vessel. Looking at the geometrical 3D object spanned by the eigenvectors, it deforms from a sphere (Figure 1, left) into an ellipsoid (Figure 1, right), as function of the vesselness response. Between these extremes, the sensitivity on the vesselness response $\mathcal{V}$ can be adjusted by the parameter s as shown by the graph in Figure 1. Values of s above one increase the sensitivity, and values below one decrease the sensitivity. This sensitivity parameter does not alter the smoothness property of the vesselness function. Furthermore, the Hessian and the smoothed vesselness function are calculated on the evolving image, yielding nonlinear diffusion. Other definitions yielding other scale spaces are also possible - in previous work (Manniesing and Niessen, 2005) we defined D as given by Equation 10, but Λ' having the following functions on its diagonal: $\lambda'_1 \triangleq \epsilon + (1 - \epsilon) \cdot \mathcal{V}$ and $\lambda'_{\{2,3\}} \triangleq \epsilon$. That is, for all structures diffusion is small and isotropic, except within a vessel where the vesselness is high and diffusion is maximal in the minimal curvature direction. The new definition is more appropriate since it exhibits stronger diffusion for both vessel and non-vessel structures, stronger anisotropic diffusion for vessel structures and includes nonlinear behavior on $\mathcal{V}$ as is shown in Figure 1b. The new definition satisfies the filter conditions mentioned in Section 2.1.

3 Experimental Framework

We applied vessel enhancing diffusion in various settings, studying its visualization aspects in patient data, the effect on diameter measurements in phantom data and the potential as preprocessing step in cerebral vessel segmentation. For a better characterization of the method, VED is compared to other well established diffusion filtering techniques. This section introduces the experimental framework. This includes CTA data acquisition (Section 3.1), the different diffusion filters (Section 3.2) and the parameter settings (Section 3.3).

[2] Large values for ω should be accompanied by smaller time discretization steps in order to prevent instabilities.

3.1 Data Acquisition

The method is applied to phantom and patient data. The phantom that is used is a 3D cerebrovascular life-sized flow phantom with known diameters (Fahrig et al., 1999). The phantom models the most important cerebral vessels, including the feeding arteries (Internal Carotid Arteries and Vertebral Arteries) and the Circle of Willis. The diameters vary in the range $[1.0, 3.5]$ mm, and average diameters and lengths have been taken from literature to model the vessels. Furthermore, twelve cerebral CTA patient data sets are randomly selected from the Department of Radiology of the University Medical Center Utrecht. Both phantom and patient data have been acquired on a 16-slice scanner (Philips Mx8000) and consist of approximately 300 slices (512×512) with an in plane resolution of 0.3125 mm $\times$ 0.3125 mm and slice spacing of 0.5 mm. For the patient data a second, low dose non-contrast enhanced scan is acquired which is rigidly registered to the original contrast enhanced scan. The bone structures are then segmented by thresholding and used to mask the bone in the contrast enhanced scan. For further details we refer to (Venema et al., 2001) in which this technique was first introduced, and to (Manniesing et al., 2006) where bone masking was used to facilitate the segmentation of the cerebral vasculature.

3.2 Diffusion Filters

In the following the different filtering techniques to which we compare vessel enhancing diffusion are briefly described. They essentially differ only in the diffusion tensor $D : \mathbb{R}^{3\times3} \to \mathbb{R}^{3\times3}$, or *conductivity coefficient* $g : \mathbb{R} \to \mathbb{R}$ which is used in the diffusion equation $L_t = \nabla \cdot (D\nabla L)$ or $L_t = \nabla \cdot (g\nabla L)$.

Gaussian Filtering (GF) If D equals the identity matrix, we obtain the heat equation $L_t = \nabla \cdot (I\nabla L) = \Delta L$. The solution at time t is given by convolution with a Gaussian with standard deviation $\theta = \sqrt{2t}$.
Regularized Perona-Malik (RPM) Perona and Malik (1990) introduced nonlinear diffusion by making the conductivity coefficient a decreasing function of the image gradient, to limit diffusion at edges. We use the regularized version (Catté et al., 1992) $L_t = \nabla \cdot (g(||\nabla_\theta L||^2)\nabla L)$. Following (Weickert, 1996a) the conductivity coefficient g is taken as

$$g(s) \triangleq \begin{cases} 1 & s \leq 0 \\ 1 - e^{\frac{-3.31488}{(s/C)^4}} & s > 0 \end{cases} \tag{13}$$

with $s \triangleq ||\nabla_\theta L||^2$ the gradient magnitude and C the contrast parameter.
Edge Enhancing Diffusion (EED) Weickert (1996a) included orientation in the diffusion process, achieving anisotropic behavior of the diffusion. To this end, the *structure tensor* is used $J_\rho \triangleq G(\rho) * \nabla_\theta L \nabla_\theta L^T$. By the following ordering $\lambda_1 \geq \lambda_2 \geq \lambda_3$, v_1 denotes the orientation with highest intensity variation. We take $\rho = 0$ which makes v_1 parallel to $\nabla_\theta L$. The diffusion tensor is then defined as $D \triangleq Q\Lambda' Q^T$, with $\lambda'_1 \triangleq g(s)$ and $\lambda'_{\{2,3\}} \triangleq 1$ and with $g(s)$ as given in (13). In this way, diffusion perpendicular to an edge is inhibited, but *along* the edge diffusion still takes place, which is in contrast with RPM.
Coherence Enhancing Diffusion (CED) CED was proposed by Weickert (1999). By ordering the eigenvalues $\lambda_1 \geq \lambda_2 \geq \lambda_3$ of J_ρ, v_3 corresponds to the orientation with lowest variations, also called the *coherence orientation*. The degree of coherence is expressed by $\kappa \triangleq (\lambda_1 - \lambda_2)^2 + (\lambda_2 - \lambda_3)^2 + (\lambda_3 - \lambda_1)^2$. The diffusion tensor is then defined as $D \triangleq Q\Lambda' Q^T$, with $\lambda'_{\{1,2\}} \triangleq \epsilon$ and

$$\lambda'_3 \triangleq \begin{cases} \epsilon & \text{if } \kappa = 0 \\ \epsilon + (1-\epsilon) \cdot e^{-\frac{C}{\kappa}} & \text{otherwise} \end{cases} \tag{14}$$

with ϵ ensuring the positive definiteness of the tensor, and C the contrast parameter. For $\kappa > C$, λ'_3 goes to one and we have strong anistropic diffusion in the coherence orientation. For $\kappa < C$ we have small isotropic diffusion.

3.3 Parameters

Parameters are based on values reported in literature and pilot experiments, and are kept fixed in all studies except for the evolution time t. RPM, EED and CED have gradient scale $\theta = 0.2$ mm in order to capture the smallest vessels in the image, contrast $C = 80$ HU, and time discretization step $\Delta t = 0.02$. Furthermore, CED has $\rho = 1.0$ mm and $\epsilon = 10^{-2}$. For VED, following (Frangi et al., 1998), the smoothed vessel filter has parameters: $\alpha = \beta = 0.5$, and $\gamma = 5$. Furthermore, $c = 10^{-6}$ (Equation 7) , $\sigma_{min} = 0.2$ mm and $\sigma_{max} = 2.0$ mm, with 10 different scales, exponentially distributed between σ_{min} and σ_{max}. Diffusion is performed with $\omega = 25$ and $s = 5.0$ (Equation 11), $\epsilon = 10^{-2}$ (Equation 12), and time step $\Delta t = 10^{-3}$.

4 Vessel Enhancement

First the effect of VED on vessel enhancement is studied. Visualization aspects are described in Section 4.1, noise filtering of low dose CT data is treated in

Section 4.2 and a comparison with a vesselness filter without diffusion is made in Section 4.3.

4.1 Visualization Aspects

The most obvious application of VED is noise reduction while preserving vessel structures, e.g. for improved visualization, or as a multiscale approach to vessel image analysis. There are three characteristic aspects of vessel enhancement. First, its capability of enhancing the continuity of vessel segments, second, the improvement in separation of (overlapping) vessels in maximum intensity projections (MIPs), and third, its effective blurring of background or non-vessel like structures.

Improved continuity of vessels may be beneficial for e.g. vessel tracking, central vessel axis tracking or for segmentation algorithms that start growing from initial points within the vessels. Owing to the strong anisotropic behavior on the vesselness response, VED is capable of overcoming significant intensity drops along the vessel, see Figure 2 for two examples of a vessel lying in the foreground (arrow 1) and a vessel lying in the background (arrow 2). The middle image in Figure 2 shows that VED also leads to improved vessel separation. In MIPs, vessels with almost similar intensity values will show overlap. Since filtering results in smoothing along the vessel trajectory, each individual vessel will have a much more homogeneous intensity distribution,

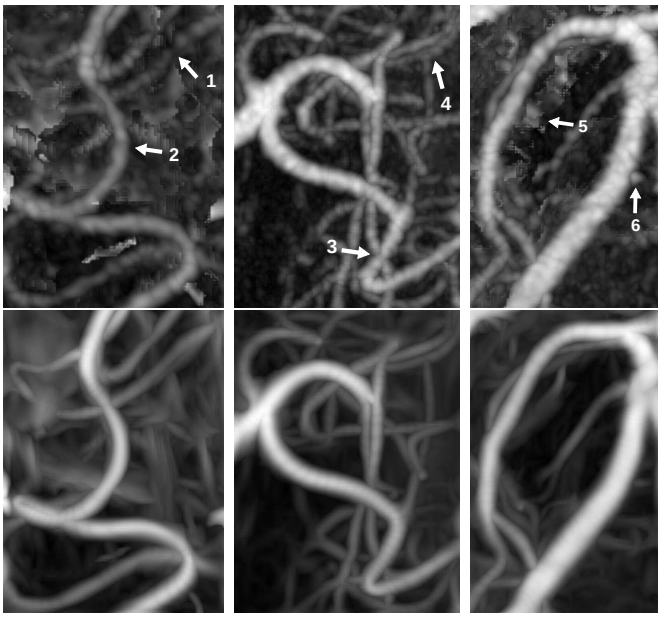

Fig. 2. Three pairwise axial MIPs of the original (top row) and the filtered data (bottom row) after $n = 40$ iterations. Arrows indicate vessel segments of interest, see Section 4.1.

while the small gap between vessels become more pronounced (arrow 3). Also, because of the strong anisotropic blurring and the multiscale character of the filter, noisy small vessels lying in close proximity to each other can better be distinguished after filtering (arrow 4). Finally, it can be observed that VED leads to excellent background suppression which is due to the strong isotropic blurring for non-vessel structures. For example, arrow 5 points at an artifact resulting from the bone masking stage. VED identifies these structures as not being tube shaped, and filters them out. Arrow 6 is an example of a high intensity valued structure that is smoothed out since it resembles a blob more than a tube (condition B given by Equation 3).

4.2 Low Dose CTA Noise Filtering

A particularly useful application is noise filtering of low dose CT scans. In CT imaging, X-ray exposure poses a risk to the patient. Attempts to lower this risk usually comes at the expense of a degraded image quality. Two out of the twelve data sets used in the presented study were scanned at approximately half the dose of the standard setting of the CT head protocol of 440 mAs. The data sets have the same dimensions and voxel sizes as the normal dose data sets. The resulting loss in image quality is significant, as can be seen in the first and third frame of Figure 3, and may hamper interpretation and automated analysis. The results of filtering are shown next to them and show most convincingly that VED is capable of enhancing tube like structures while suppressing image noise.

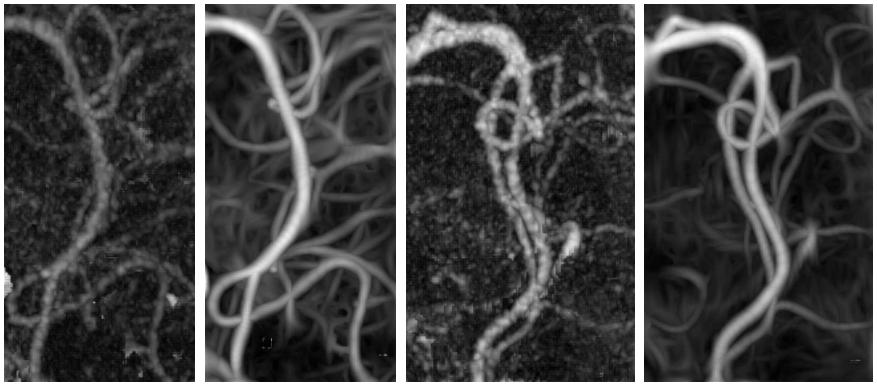

Fig. 3. Two regions of interests from low dose CT scans (first and third frame). The filtered results after $n = 40$ iterations are shown next to them. It is convincing on how VED is capable of enhancing tube like structures in the image data.

4.3 Comparison with Vesselness Filter

The vesselness filter as introduced by Frangi et al. (1998) was aimed at vessel enhancement in the image. However, applying a local filter is a substantially different approach compared to a vesselness measure into a diffusion framework. To compare both approaches an experiment was performed using the same parameter settings. In Figure 4 it can be observed that the shrinkage effect of the vesselness filter is not present in VED (arrow 1 and arrow 3). Shrinkage is due to the increasing deviation from a tube like structure when approaching the boundaries of the vessel. Furthermore, VED has better performance with respect to background blurring compared to vesselness filtering (arrow 2 and arrow 4).

5 Scale Space Comparison with Diffusion Filters

In this section scale spaces constructed with VED and different existing diffusion filters (GF, RPM, EED and CED) are compared. Owing to the different conductivities in the various implementations, these scale spaces can not be compared using the evolution time. Therefore, we use an information theoretical approach (Niessen et al., 1997). This approach is based on the classical entropy measure or Shannon entropy (Shannon, 1948), given by $H(L) \triangleq -\sum_I p \log p$ with I denoting the spatial image domain and with p

$$p \triangleq \frac{L(t)}{\sum_I L(t)} \tag{15}$$

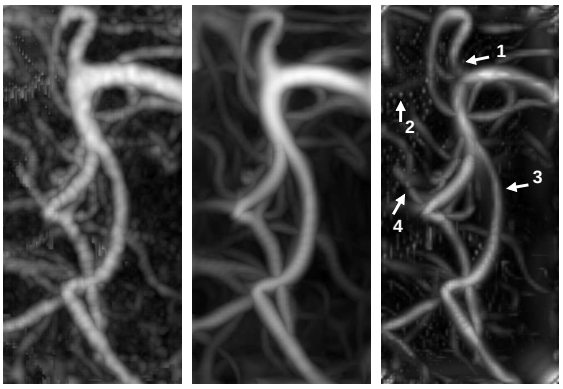

Fig. 4. A comparison between VED and the vesselness filter. The original data is shown in the first frame, the result of VED in the second frame and the result of vesselness filtering in the third frame. Arrows indicate points of interests, see Section 4.3.

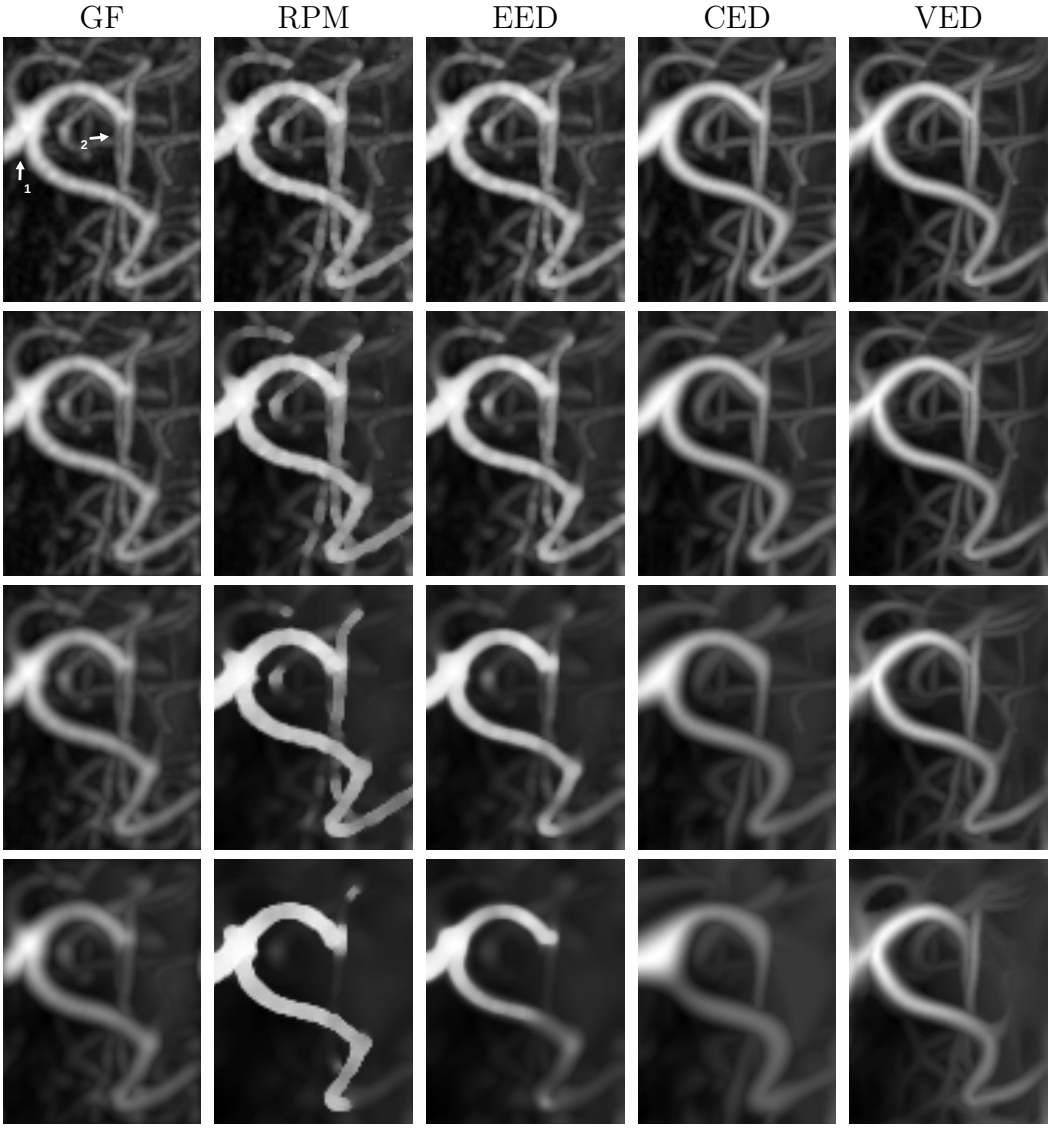

Fig. 5. A comparison between scale spaces. The original data is shown in the second example of Figure 2b. Each column shows the results of one diffusion method, each row shows the results for the same time value T (Equation 16). For discussion see Section 5.

It can be shown that H is a monotonically growing function for increasing diffusion (Sporring, 1996). We now define the normalized time T as follows

$$T \triangleq \frac{H(L_t) - H(L_0)}{H(L_\infty) - H(L_0)} \tag{16}$$

with range $T \in [0, 1]$. Since L_∞ is the final steady state image it follows that the maximum entropy $H(L_\infty)$ is given by $\log N$, with N the image dimension. In order to effectively compare different scale spaces, we align them based on the normalized time T.

Results for a normal dose CT scan (Figure 2, second example) are shown in Figures 5. Looking at the first rows of both figures, showing the results for a very small T, it is clear that both CED and VED already achieve good noise suppression compared to the other methods. Furthermore, for increasing T, VED tends to enhance tube like structures, an effect that is most clearly visible with vessel bifurcations (arrow 1) or other non tubular structures. Eventually, the vessels are smoothed out or are becoming smaller for GF, CED and VED, while RPM and EED retain the width of the vessels much better. If we would zoom in on the results of RPM and EED (not shown here) the noise on the edges are preserved by RPM and reduced by EED, as was expected. In general, VED has better preservation of smaller vessels (arrow 2) compared to other filters, but tends to make non tubular structures more tubular shaped (arrow 1).

6 Diameter Quantification

The scale space comparison presented in Section 5 gives a first insight in the differences in behavior between the diffusion filters. In order to provide a quantitative evaluation a diameter study on phantom data is carried out. The purpose of this study is to investigate the influence of filtering on diameter measurements at different levels in scale space.

For this study a cerebrovascular phantom with known diameters varying in the range 1.0 to 3.5 mm is used (Section 3.1). First, 17 seed points are placed in the different arteries forming the Circle of Willis (CoW) and in the different arteries feeding the CoW. The diameter quantification approach is based on intensity thresholding for segmentation and proceeds following the steps described in (Manniesing et al., 2006). In order to compare the measurements to ground truth a Bland and Altman (1986) analysis is performed, which gives a bias and standard deviation (we subtract the measurement from ground truth). For each diffusion filter we vary the number of iterations, thereby building the scale space. For approximately 25 scale levels the diameter quantification algorithm is carried out. This gives for each point a bias and standard deviation as function of scale. Finally, all scales are normalized according to Equation 16.

The results are shown in Figure 6. At time zero the measurements of all filters correspond with an error of 0.05 ± 0.31 mm. When increasing time, VED and CED best preserve the diameter of the vessel as can be seen by the smaller bias. However, for CED the bias drops quickly and fluctuates strongly for $T > 20$. RPM has the least amount of diffusion along the edges, and therefore affects the boundary positions the least (see also Figure 5). The strong decrease in bias is the result by our intensity based segmentation method - for increasing

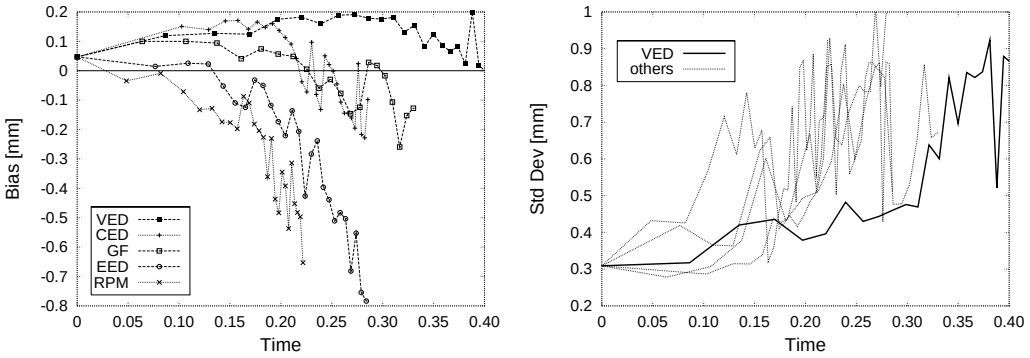

Fig. 6. The bias between ground truth and the diameter measurements of the method (figure left) and the corresponding standard deviations (figure right) as function of the synchronized time T.

time the correlation between the intensity values at the central vessel axis and the vessel width changes. The same argument applies to EED although to a lesser extent.

From the bias graph we learn that VED has a much smoother influence on the bias in time compared to other methods. From the accuracy graph we learn that all methods strongly decreases accuracy, but this trend is the slowest for VED.

7 Improved Segmentation

Finally, we evaluated VED as a preprocessing step for cerebral vasculature segmentation in 3D patient data. Segmentation is carried out by level set evolution (Osher and Sethian, 1988; Sethian, 1999). The speed function is defined by fitting Gaussian distributions on the histogram obtained from a prior selection of vessel and background intensity values. Initialization is carried out by manually placing seed points at the larger arterial vessels of interest forming the Circle of Willis. For exact details on the segmentation method we refer to (Manniesing et al., 2006), in which the level set based method was presented and applied to CTA cerebral vasculature segmentation. The segmentation method is run twice on the data sets, first on the original data and then on the filtered data, both with the same parameters and initialization points. The level sets are evolved for an arbitrarily high number of iterations and convergence was checked by visual assessment of the volume measurements. Each pair of segmentation results is then evaluated by axial MIPs according to the following criteria: (i) segmentation of the distal and smaller vessels, (ii) vein suppression near the skull base and (iii) suppression of non-vessel structures. The results of all comparisons are summarized in Table 1. In nine data sets vessel enhancing diffusion performed better at segmenting the distal and

smaller vessels, in only one case the original data had better performance. This single case concerned only a very small vessel segment (one to a few voxels) that was included at the posterior side of the Circle of Willis. With respect to falsely including veins segments into the final segmentation, VED five times outperformed no diffusion, and in two cases the results in the original data was better. With respect to suppression of non-vessel structures VED had better performance in two cases. In Figure 7 two examples of pairs of results are shown for a normal dose and a low dose scan. An example of improved distal segmentation is given by arrow 1. An example of vein suppression near the skull is given by arrow 2; in most other data sets the improvement in vein suppressing was more subtle. Generally speaking, using VED as preprocessing step leads to smoother vessels and to an effective suppression of noise and non-vessel structures, resulting in segmentation results which are as good as, and often better than the segmentation results obtained without prior diffusion.

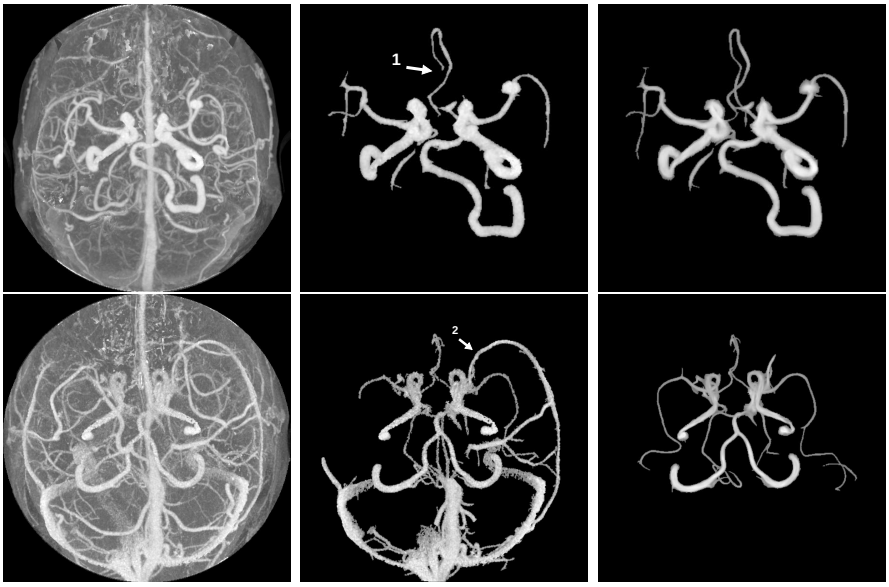

Fig. 7. Level set based segmentation on a normal dose CT scan (top row) and a low dose CT scan (bottom row). Axial MIPs are shown of the masked image, the segmentation result without prior VED and the segmentation result with prior VED.

Table 1
Comparison of level set based segmentation with and without prior vessel enhancing diffusion.

Criteria	**Original**	**VED**
Segmentation of distal and smaller vessels	1	9
Vein suppression near the skull	2	5
Suppression of non-vessel structures	0	2

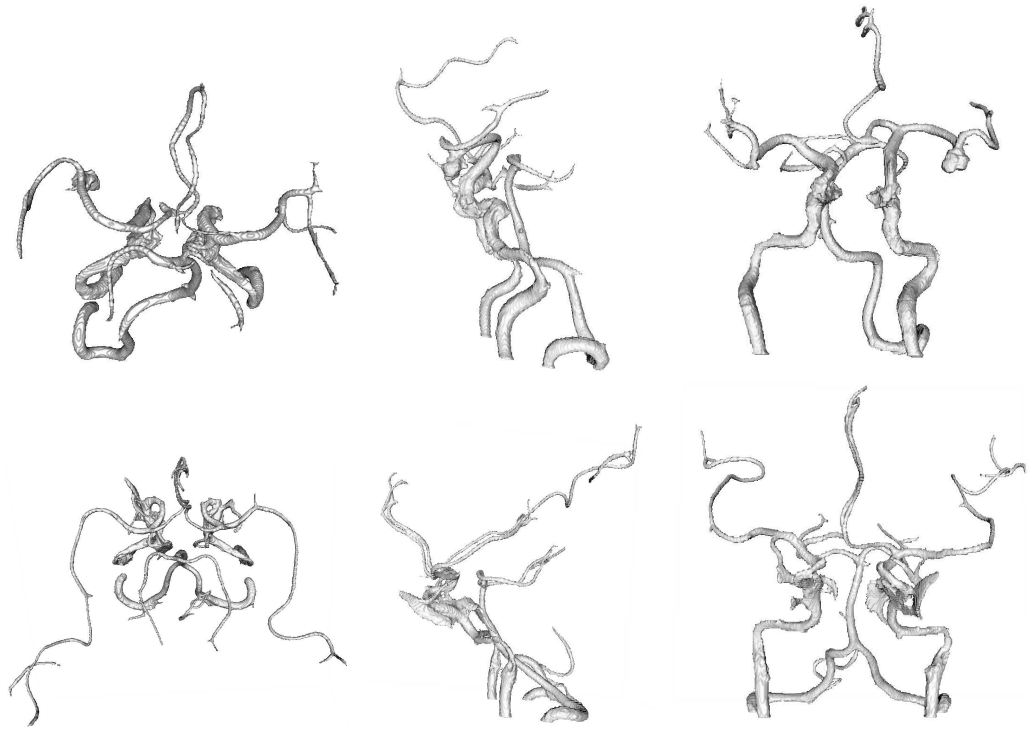

Fig. 8. Surface renderings of the segmentation results after preprocessing by VED. Axial MIPs of the original data are shown in Figure 7. Axial, sagittal and coronal view of the normal dose scan (top row), and the same views of the low dose scan (bottom row).

8 Discussion and Conclusion

A nonlinear, anisotropic, Hessian based diffusion scheme has been proposed, steered by a vesselness filter, to enhance vascular structures within the framework of scale space theory. The theoretical contribution is the modification of the vesselness function such that it becomes a smooth function on its domain. Smoothness of the vesselness function is required to have desirable scale space properties.

The method has been applied to CTA data of the cerebral vasculature and it was first shown that VED leads to improved visualization by enhancing vessel structures and reducing background. In particular, the visualization results on the low dose CT scans show very strong vessel enhancement (Figure 3), which clearly outperforms commonly used vessel filtering techniques (Figure 4). The method has then been compared to GF, RPM, EED and CED. At a low scale in scale space, CED and VED show similar improvements in vessel enhancement with the difference of CED having better preservation of non-tubular structures. For increasing scale, VED has better preservation of the smaller vessels in the image compared to all other methods. This is probably a result of the multiscale character of VED.

In order to quantify the effect of diffusion filtering on the vessel width, a diameter quantification study has been carried out on a phantom model of the cerebral vasculature. In general, the diameter measurements tend to increase, except for VED and CED at low scale. Furthermore, the accuracy was determined by which the diameters are assessed for increasing scale. We found that VED compared to the other filters maintains a higher accuracy in a large range of scales. Because of the influence on the vessel width, VED, and diffusion filtering in general, are in particular useful as preprocessing step in subsequent vessel and vessel axis detection or segmentation algorithms. We do, however, emphasize that we have introduced a scale space approach. Thus we have always access to all levels of scale, and VED is particularly useful for multiscale approaches to vessel image analysis.

We also evaluated the potential of VED as a preprocessing step for vascular segmentation. A level set based segmentation method guided by intensity information was applied to CTA cerebral vasculature segmentation, with and without prior vessel enhancing diffusion. Initialization was carried out by manually placing seed points at the larger arterial vessels and it was found that in the majority of the twelve CTA data sets, after preprocessing and without extensive parameter optimization, the propagating level set front had less difficulties in reaching the smaller and distal parts of the vasculature and more often had excluded the (smaller) veins nearby the skull in the arterial segmentation.

A final note concerns the computational issues of VED. The multiscale character of the vesselness filter and the nonlinear character of the diffusion process puts a heavy burden on the computation resources. VED applied to the full data sets (156 MByte) in the segmentation study, took on average 20 minutes per iteration on a 2.4 GHz 64 bits Linux system. However, the code has not been optimized and the vesselness function was calculated at a large number of scales. Pilot experiments have shown that reducing the number of scales is possible without compromising the visual results. Also, in many applications a region of interest can be selected. These speed up issues will have to be considered in order for the method to be used in practice.

Acknowledgments

We thank Stefan Klein and Marius Staring (Image Sciences Institute, Utrecht, the Netherlands) and Theo van Walsum (Erasmus Medical Center, Rotterdam, the Netherlands) for discussions and comments on earlier drafts of this manuscript. We thank the anonymous reviewers for their comments which led to an enhanced presentation.

References

Bland, J., Altman, D., 1986. Statistical methods for assessing agreement between two methods of clinical measurement. Lancet i, 307–310.

Cañero, C., Radeva, P., 2003. Vesselness enhancement diffusion. Pattern Recognition Letters 24, 3141–3151.

Catté, F., Lions, P.-L., Morel, J.-M., Coll, T., 1992. Image selective smoothing and edge detection by nonlinear diffusion. SIAM J. Numer. Anal. 29 (1), 182–193.

Fahrig, R., Nikolov, H., Fox, A., Holdsworth, D., 1999. A three dimensional cerebrovascular flow phantom. Medical Physics 8 (26), 1589–1599.

Frangi, A., Niessen, W., Vincken, K., Viergever, M., 1998. Multiscale vessel enhancement filtering. In: Medical Image Computing and Computer-Assisted Intervention. pp. 130–137.

Koller, T., Gerig, G., Székely, G., Dettwiler, D., 1995. Multiscale detection of curvilinear structures in 2d and 3d image data. In: International Conference on Computer Vision. pp. 864–869.

Krissian, K., 2002. Flux-based anisotropic diffusion applied to enhancement of 3-D angiogram. IEEE Transaction on Medical Imaging 21 (11), 1440–1442.

Krissian, K., Malandain, G., Ayache, N., Vaillant, R., Trousset, Y., 2000. Model-based detection of tubular structures in 3D images. Computer Vision and Image Understanding 80 (2), 130–171.

Lindeberg, T., 1998. Edge detection and ridge detection with automatic scale selection. Int. J. of Computer Vision 30 (2), 117–154.

Lorenz, C., Carlsen, I.-C., Buzug, T., Fassnacht, C., Weese, J., 1997. Multiscale line segmentation with automatic estimation of width, contrast and tangential direction in 2d and 3d medical images. In: Computer Vision, Virtual Reality and Robotics in Medicine. pp. 233–242.

Manniesing, R., Niessen, W., 2005. Multiscale vessel enhancing diffusion in CT angiography noise filtering. In: Christensen, G., Sonka, M. (Eds.), Information Processing in Medical Imaging. Vol. 3565. pp. 138–149.

Manniesing, R., Velthuis, B., van Leeuwen, M., van der Schaaf, I., van Laar, P., Niessen, W., 2006. Level set based cerebral vasculature segmentation and diameter quantification in CT angiography. Medical Image Analysis 10 (2), 200–214.

Niessen, W., Vincken, K., Weickert, J., Viergever, M., 1997. Nonlinear multiscale representations for image segmentation. Computer Vision and Image Understanding 66 (2), 233–245.

Osher, S., Sethian, J., 1988. Fronts propagation with curvature dependent speed: Algorithms based on Hamilton-Jacobi formulations. Journal of Computational Physics 79 (1), 12–49.

Perona, P., Malik, J., 1990. Scale-space and edge detection using anisotropic diffusion. IEEE Transactions on Pattern Analysis and Machine Intelligence 12 (7), 629–639.

Sato, Y., Nakajima, S., Shiraga, N., Atsumi, H., Yoshida, S., Koller, T., Gerig,

G., Kikinis, R., June 1998. Three-dimensional multi-scale line filter for segmentation and visualization of curvilinear structures in medical images. Medical Image Analysis 2 (2), 143–168.

Sethian, J., 1999. Level Set Methods and Fast Marching Methods, 2nd Edition. Cambridge University Press.

Shannon, C., 1948. A mathematical theory of communication. Bell System Technical Journal 27, 379–423/623–656.

Sporring, J., 1996. The entropy of scale-space. In: International Conference on Pattern Recognition. pp. 900–904.

ter Haar Romeny, B. (Ed.), 1994. Geometry-Driven Diffusion in Computer Vision. Vol. 1. Kluwer Academic Publishers.

Venema, H., Hulsmans, F., den Heeten, G., 2001. CT angiography of the Circle of Willis and intracranial internal carotid arteries: Maximum intensity projection with matched mask bone elimination - feasibility study. Radiology 218 (3), 893–898.

Weickert, J., 1996a. Anisotropic diffusion in image processing. Ph.D. thesis, University of Kaiserslautern.

Weickert, J., 1996b. Theoretical foundations of anisotropic diffusion in image processing. In: Theoretical Foundations of Computer Vision. pp. 221–236.

Weickert, J., 1997. A review of nonlinear diffusion filtering. In: ter Haar Romeny, B., Florack, L., Koenderink, J., Viergever, M. (Eds.), Scale-Space Theory in Computer Vision. Vol. 1252 of Lecture Notes in Comp. Science. Springer, pp. 3–28.

Weickert, J., 1999. Coherence-enhancing diffusion filtering. International Journal of Computer Vision 31, 111–127.